Mon. Not. R. Astron. Soc. **418,** 1272–1284 (2011) doi:10.1111/j.1365-2966.2011.19579.x

Effect of different stellar galactic environments on planetary discs – I. The solar neighbourhood and the birth cloud of the Sun

Juan J. Jiménez-Torres,[1] Barbara Pichardo,[1⋆] George Lake[2] and Henry Throop[1,3]

[1]*Instituto de Astronomía, Universidad Nacional Autónoma de México, Apdo. postal 70-264 Ciudad Universitaria, DF, Mexico*
[2]*Institute for Theoretical Physics, University of Zürich, CH-8057 Zürich, Switzerland*
[3]*Department of Space Studies, Southwest Research Institute, 1050 Walnut Street, Ste 300, Boulder, CO 80302, USA*

Accepted 2011 August 2. Received 2011 June 27; in original form 2010 June 10

ABSTRACT

We have computed trajectories, distances and times of closest approaches to the Sun by stars in the solar neighbourhood with known position, radial velocity and proper motions. For this purpose, we have used a full potential model of the Galaxy that reproduces the local z-force, the Oort constants, the local escape velocity and the rotation curve of the Galaxy. From our sample, we constructed initial conditions, within observational uncertainties, with a Monte Carlo scheme for the 12 most suspicious candidates because of their small tangential motion. We find that the star Gliese 710 will have the closest approach to the Sun, with a distance of approximately 0.34 pc in 1.36 Myr in the future. We show that the effect of a flyby with the characteristics of Gliese 710 on a 100 au test particle disc representing the Solar system is negligible. However, since there is a lack of 6D data for a large percentage of stars in the solar neighbourhood, closer approaches may exist. We calculate parameters of passing stars that would cause notable effects on the solar disc. Regarding the birth cloud of the Sun, we performed experiments to reproduce roughly the observed orbital parameters such as eccentricities and inclinations of the Kuiper belt. It is now known that in Galactic environments, such as stellar formation regions, the stellar densities of new born stars are high enough to produce close encounters within 200 au. Moreover, in these Galactic environments, the velocity dispersion is relatively low, typically $\sigma \sim 1$–$3\,\mathrm{km\,s^{-1}}$. We find that with a velocity dispersion of $\sim 1\,\mathrm{km\,s^{-1}}$ and an approach distance of about 150 au, typical of these regions, we obtain approximately the eccentricities and inclinations seen in the current Solar system. Simple analytical calculations of stellar encounters effects on the Oort Cloud are presented.

Key words: Kuiper belt: general – Oort Cloud – stars: kinematics and dynamics – solar neighbourhood.

1 INTRODUCTION

Observations of extrasolar planets (e.g. Schneider 2010) show that planetary orbits in other planetary systems are disordered, showing a wide range of eccentricities. For extrasolar planets with semimajor axes $a \geq 0.1$ au, the mean of the eccentricity distribution is $e \approx 0.3$ and the median is $e \approx 0.24$ (Adams 2010). Thus, available data indicate that planetary systems discovered in the last decade are more dynamically active and disordered than our own (Udry & Santos 2007; Adams 2010).

A study of planetary disc dynamics under the stellar influence of different Galactic environments is presented in a set of papers. In this work, we introduce the first two Galactic environments related to the Sun: the solar neighbourhood and the birth cloud of the Sun.

⋆E-mail: barbara@astroscu.unam.mx

The solar neighbourhood has been defined as the region of space centred on the Sun that is much smaller than the overall size of the Galaxy, and whose contents are known with reasonable completeness (Gilmore 1992; Binney & Tremaine 2007). Now, from a theoretical simple approximation, it seems clear that the probability in the current solar neighbourhood to have an important encounter for the planetary system, with another star (i.e. less than 300 au for a solar mass stellar flyby), is almost negligible. Let us, for example, consider a typical stellar density for the solar neighbourhood of approximately $0.05\,\mathrm{M_\odot\,pc^3}$, we can calculate the mean free path, λ, for approaches within say 300 au, as the radius of a cross-section, σ, and setting $50\,\mathrm{km\,s^{-1}}$ as the typical velocity dispersion, σ_v, in the solar neighbourhood, we find that the time necessary, in the current conditions of velocity dispersion and density of the solar neighbourhood, to see an encounter within 300 au with the Sun (or between any couple of stars in these dynamical conditions) would be $t \approx \lambda/\langle v\rangle \approx 1/\sigma n \sigma_\mathrm{v}$, which corresponds to approximately three

Hubble times. On the other hand, García-Sánchez et al. (2001), by comparing *Hipparcos* observations with the stellar luminosity function for star systems within 50 pc of the Sun, estimate that only about one-fifth of the star systems were detected by *Hipparcos*, and they correct for that incompleteness in the data obtaining about 12 stellar encounters per Myr within 1 pc of the Sun.

However, in the case of the Solar system it is clear that a rough approximation is not good enough. Thanks to *Hipparcos*, and some knowledge of the local and global Galactic potential we are now able to compute orbits, within a few million years, of neighbouring stars and determinate at good approximation distances, times, etc. to stars in the solar neighbourhood. This will improve enormously in the near future with the advent of large surveys of the Milky Way such as *GAIA*. For now, we are not close to having a complete set of 6D parameters (position and velocity) of all stars near the Sun. In this paper, we take the nearest stars to the Sun with proper motions, parallaxes and radial velocities, and we compute their past and future trajectories as well as their closest approach, distance and time. Thus, for our purposes, the solar neighbourhood is the radius of the sphere that contains all the stars (with 6D parameters known), whose maximum approach to the Sun was or will be less than 5 pc within 10 Myr to the past or to the future; this is approximately 200 pc.

On the other hand, even when, in the current solar neighbourhood conditions, the probability of close stellar approaches is almost negligible, it is now known that as many as 90 per cent of stars appear to form in clusters or groups with 10^2 to 10^3 members (Carpenter 2000; Lada & Lada 2003; Clark et al. 2005; Adams 2010). Short-lived radioisotopes in solar meteorites argue that formation happened near at least one massive star, probably in a large cluster (Goswami & Vanhala 2000; Meyer & Clayton 2000; Hester et al. 2004; Looney, Tobin & Fields 2006; Wadhwa et al. 2007). In their early stages, most stars were in relatively crowded environments. In such environments, close stellar encounters would be frequent and affect the stability of planetary systems around the stars (de la Fuente Marcos & de la Fuente Marcos 1997; Laughlin & Adams 1998; Hurley & Shara 2002; Pfahl & Muterspaugh 2006; Spurzem et al. 2009).

Some work has been devoted to searching for stellar perturbers of the cometary discs and clouds. Mathews (1994) identified close approaches for six stars within the next 5×10^4 yr, within a radius of about 5 pc. García-Sánchez et al. (1997) started a search for stars passing close to the Sun using *Hipparcos* data, assuming a straight-line motion model. Subsequently, García-Sánchez et al. (1999) continued their search by integrating the motion of the candidate stars and the Sun in a local Galactic potential and in a simple global Galactic potential. More recently, Bobylev (2010) presents a study of the closest encounters of stars in the solar neighbourhood with the Sun, using also a simple local approximation to integrate orbits.

Of course, a star passing near the Sun has greater effect on the Oort Cloud – an extremely extended structure – than on the planetary disc. However, in the Solar system, the Kuiper belt has properties acquired early in its history, and some of these are difficult to explain under the assumption that the Solar system has always been isolated, such as the excitation of the eccentricities and inclinations in the classic belt, the mass deficit of the Kuiper belt and the sharp outer edge of the classical belt at approximately 48 au. Beyond this boundary, only high-eccentricity objects typical of the scattered disc or of the detached population seem to exist, and finally, some mysterious large bodies (approximately Pluto size) exist, with extreme eccentricities and perihelia (Sedna). One of the most accepted theories to explain the characteristics of Kuiper belt is then based on the idea that a close stellar passage could have taken place in the early history of our planetary system (Ida, Larwood & Burkert 2000; Kobayashi & Ida 2001). In this paper, we experiment with stellar encounters on a 100 au particle disc, looking for the minimum distance where an encounter is important, and we seek to produce Kuiper belt orbital characteristics such as eccentricities and inclinations.

This paper is organized as follows. In Section 2, we describe the methods and numerical implementation. In Section 3, we present the stellar sample of the solar neighbourhood and our results for this first Galactic environment. In Section 4, we show the results of the Sun's birth cluster. Conclusions are presented in Section 5.

2 METHODOLOGY AND NUMERICAL IMPLEMENTATION

We have implemented two codes to solve the equations of motion. The first calculates stellar trajectories in the solar vicinity with all their observational orbital parameters known (positions and velocities) in a Milky-Way-like potential. The second simulates debris discs under the influence of stellar encounters.

2.1 The solar neighbourhood code

We calculate the trajectory of stars with the known 6D data (derived from α, δ, radial velocity and proper motions known) to determinate the distance and time (past or future) of their closest approach to the Sun.

Instead of using a straight-line approximation to solve the stellar orbits in the solar neighbourhood, we solved the orbits in a Milky-Way-like Galactic potential (Pichardo et al. 2003; Pichardo, Martos & Moreno 2004).

The axisymmetric part of the model consists of a background potential with a bulge, a flattened disc (Miyamoto & Nagai 1975) with a scaleheight of 250 pc and a massive halo extending to a radius of 100 kpc. The model has a total mass of 9×10^{11} $M_\odot$, with a local escape velocity of 536 km s^{-1}. This potential satisfies observational constraints such as the Galactic rotation curve, with a rotation velocity of 220 km s^{-1} at $R_0 = 8.5$ kpc, the perpendicular force at the solar circle and the Oort constants, among others (for more details see Pichardo et al. 2003, 2004; Martos et al. 2004; Antoja et al. 2009).

Given data in the equatorial system are transformed to Galactic coordinates. The equations of motion are solved with a Bulirsh–Stoer adaptive integrator (Press et al. 1992) that gives relative errors for the integrals of motion (total energy, z-component of angular momentum, for the axisymmetric potential, or Jacobi constant, for the barred or armed potential) of 10^{-10} in the worst case (when the non-axisymmetric components of the Galaxy are included). The Sun is located 8.5 kpc from the Galactic nucleus and 0.035 kpc above the plane of the disc. The velocity along the x-axis is -9 km s^{-1} and on the y-axis is -220 km s^{-1}.

This code computes distances, times, velocities and uncertainties for stars at the moment of maximum approach to the Sun within observational uncertainties. These are obtained from catalogues and data mainly based on Simbad, *Hipparcos* and Nexxus 2, and papers Bower et al. (2009), Dybczyński (2006) and García-Sánchez et al. (1999). Initial conditions are constructed as normal random values within observational uncertainties (note that it is the uncertainty in parallax the one with the normal distribution, not the uncertainty

in distance). 10 000 orbits were computed as initial conditions for each star in order to obtain the final error bars.

In the original version of the code, additionally to the background axisymmetric potential, it included non-axisymmetric features: spiral arms and bar (Pichardo et al. 2003, 2004). In the same way as García-Sánchez et al. (2001), who constructed a potential including a very simple axisymmetric background and weak spiral arms (pitch angle of $\sim 6.^{\circ}9$), we conclude that the difference between using a full Galactic model and an axisymmetric model among the solar neighbourhood stars is negligible (within $\approx$3 per cent for the most distant stars to the Sun in this study). Although there is evidence that the existence of spiral arms and bars has direct influence on the local stellar distribution and evolution (Dehnen 2000; Chakrabarty 2007; Antoja et al. 2009), the time we run the orbits is rather short ($\leq 10^7$ yr), much less than a dynamical time, and not enough to produce a notable difference in the orbits produced by the non-axisymmetric potential. To facilitate the calculations we performed the final calculations only with the axisymmetric background potential of the Galaxy, since the bar and arms are not of importance in this time-scale.

2.2 The stellar encounter code

The second code is a 3D particle code that calculates the interaction of a planetary system (a central star and a disc of test particles) with a second stellar body (a flyby star).

The sampling of test particles goes as $a \propto n^{-3/2}$, where a is the initial radius of a particle orbit and n is the number of the orbit; these test particles are affected by the gravitational forces of both the central star and the flyby star, and the equations of motion are solved for the central stars (Suns) non-inertial frame of reference. The code calculates the main orbital characteristics of each of the test particles simulating a debris disc after the flyby; it calculates the semimajor axis, the eccentricity and the inclinations. The Bulirsh–Stoer integrator gives a maximum relative error before the flyby of 10^{-14} and 10^{-13} in the energy and angular momentum integrals, respectively.

In Fig. 1, we show the schematics of the relevant parameters used on the code of a stellar encounter. The dark disc at the centre of the system represents the planetary disc, the grey sphere represents the radius of the minimum distance of the flyby and the bright disc is tangent to the sphere at the point of minimum distance. The flyby attack angles are: ϕ, the azimuthal angle with respect to the disc, it goes from 0° to 360°; θ, the polar angle with respect to the disc, goes from -90° to 90°; and α, the angle between the flyby plane orbit and the symmetry axis of the planetary disc, it goes from 0° to 360°.

With the purpose of covering several Galactic stellar environments, and to acquire a physical idea of what parameters are the most relevant in this kind of interaction, besides the specific applications of this code to the Sun's birth cluster and the current solar environment, we computed more than a thousand experiments covering the different Galactic ranges in distance (stellar closest approximation), velocities, angles of flyby trajectories and stellar masses. For distance: 5 to 1000 au, for velocity: 1 to 180 km s^{-1}, for mass: 1 Jupiter mass to 4 $M_{\odot}$. Regarding the flyby attack angle ϕ, due to the symmetry of the problem, this entrance angle is indistinct; we took for our experiments $\phi = 0^{\circ}$.

In the application presented in this paper the effects of the exact direction of the entrance of the flyby resulted of no importance, this, due to the fact that: (a) in the current solar neighbourhood stars will not come close enough for the angle to be important and the effect of encounters at such large distances would be negligible, even for objects in the Oort Cloud in the majority of cases; (b) in the case of the birth cloud of the Sun, stars' approaches might have been important; however, in this case the orientation of discs with respect to flybys is unknown and probably rather random.

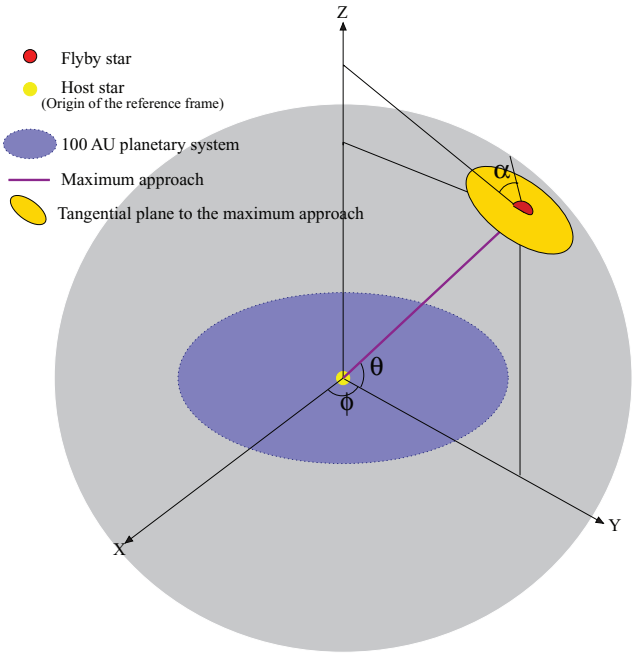

Figure 1. Schematic figure of a stellar encounter on a planetary system by a flyby star. The disc is simulated with test particles. The initial conditions are particles on circular orbits with zero inclination.

Since we are talking about one single encounter in this Galactic environment, we choose a general interaction, this is 45° for θ and α, that should produce an intermediate effect produced by all possible inclinations of the orbital plane. This means, the flyby orbit will enter at 45° with respect to the plane of the disc, and 45° with respect to the disc axis. It is worth mentioning that the results are nearly insensitive to changes of α, while changes in θ produce different results being larger for $\theta = 0^{\circ}$. A global study of the parameters will be presented in a future paper.

3 RESULTS

Here, we present the first two Galactic regions studied in this work.

3.1 The solar neighbourhood

For the solar neighbourhood, we looked for the closest stars to the Sun with the known position, radial velocity and proper motions. It is worth mentioning that for the nature of the sample, we are only able to compute stars with the known 6D parameters from the literature; our sample is biased to the closest, more massive stars with the largest proper motion. However, this bias actually represents the most important candidates to perturb our planetary disc. Considering this bias, from more than a thousand stars in the full sample, we find that 67 stars passed or will pass within 3 pc from the Sun; between the last 8 Myr and the next 5 Myr, this is roughly, 5 stars Myr^{-1}. Only one of these 67 sets will barely perturb the outer Oort Cloud, and the planetary disc will not notice that star in the dynamical sense. On the other hand, it should be noted that there could be a star of which we do not have 6D information that could

come even closer than GJ 710. Even in our sample, we could have stars that will approach to the Sun several times along the stellar trajectories around the Galaxy, but in this case, there is no model of the Galaxy that is good enough to warranty precise orbits for these stars for more than a few million years.

3.1.1 The stellar sample

We used parallax and proper-motion data and uncertainties from the *Hipparcos* catalogue for 1167 nearby stars suspected to pass close to the Solar system. We take radial velocity measurements from different catalogues (*Hipparcos*, Simbad and Nexxus2) and papers (García-Sánchez et al. 1999; Dybczyński 2006; Bower et al. 2009) to produce 6D trajectories of the whole sample of stars and calculate the distance at the point of maximum approach to the Sun, the time and velocity (the whole table is available on request via an e-mail). From this sample, we produced a subsample of 67 stars with their observational uncertainties and calculated closest approach distances to the Sun, within 3 pc. From this subsample, we ran 34 stars towards the past (those receding now), and 33 stars towards the future (those approaching now) looking for those passages that might perturb on the Solar system. In particular, these 67 stars are potential perturbers of the Oort Cloud (García-Sánchez et al. 1999).

The stars with the closest approach distances, within 3 pc from the Sun, are listed in Tables 1 and 2 sorted first by receding versus approaching then by parallax. Columns are arranged as follows, star's name, parallax, radial velocity, minimum approach distance to the Sun, approach time and relative velocity. These predicted passages are contained in a time interval of about -8 and 4 Myr. The close-approach distances versus time are shown in Fig. 2. In the upper panel of this figure we show the variation with time of the separation distance between each star and the Sun, at the moment of maximum approach, for all stars in our sample (of 1167 stars), whose closest distance is less than 30 pc. The lower frame is a zoom that shows the stars with the closest approach distances, within 3 pc (Tables 1 and 2), for the time interval from -8 to 4 Myr. Stars within 2–3 pc may perturb the Oort Cloud. The star with the closest future approach is Gliese 710. The predicted minimum distance for this star is 0.34 pc in 1.36 Myr. This is the only star in the sample with an approach distance less than the radius of the Oort Cloud $\sim$0.48 pc.

3.1.2 The most interesting candidates

From this sample, if we ignore the uncertainties, we could conclude that none of these stars would approach to the Sun closer than $\sim$70 000 au (more than 200 times beyond than necessary to start affecting the outskirts of our planetary system). We have considered, however, observational uncertainties in this work. The stars that may produce important (even dangerous) approaches to the Sun are those whose tangential velocities are potentially zero (simultaneously in α and δ). We will then check on those stars whose tangential velocities (or approach distance to the Sun) are consistently zero at 3σ. This includes both stars with small tangential velocity and those with uncertain tangential velocities. This makes a total number of 12, eight to the past and four to the future, from the whole sample of 67 objects.

For these 12 stars (labelled with an asterisk in Tables 1 and 2), we have separately produced in Figs 3 and 4 histograms, eight to the past and four to the future. In each histogram we computed 10 000 random realizations with a normal distribution for the initial conditions within all the observational uncertainties, with the notable exception of the parallax, where the value was restricted to positive values. In these histograms, we analyse the most likely approach distance of Sun–star towards the past and future, respectively. All diagrams were done with the same bin size of 0.01 pc and x-axis, to better see differences between the stellar approaches.

The number of approaches closer than 0.01 pc is of 3 to the past and 8 to the future; this is equivalent to the probability of 0.03 per cent to the past and 0.08 per cent to the future of an approach to less than 0.01 pc. A more interesting distance is of course the one that could cause a notable effect on the planetary disc, and that we know now is approximately of 300 au, as we will show in Section 3.1.4. The probability of a closer than 300 au approach is then $\sim$0.0017 per cent from the eight stars to the past and $\sim$0.0006 per cent from the four stars to the future. The probabilities of these stars to pass close enough to the Solar system to affect the planetary disc are extremely low; this is true even for the star that will approach the closest (GJ 710).

3.1.3 Comparison between the straight-line approximation, local and global potentials

Following García-Sánchez et al. (2001), we compare stellar orbits with our global potential to those using the straight-line approximation and a local potential approximation from their paper. For distances of the stars larger than 50 pc the local and straight-line approximations give important differences with respect to a global model, even with times as short as 1 Myr.

García-Sánchez et al. (2001) concluded that within a time interval of $\pm$10 Myr from the present time, the predicted encounters are fairly well determined for most of the candidate stars. They are not altered significantly by the use of alternative Galactic potential models or by varying the plausible values of the Galactic parameters. The most interesting result is the future passage of Gliese 710 through the outer Oort Cloud. This result is in good agreement with the predictions using other Galactic potential models; the prediction of this stellar passage is not model dependent owing to its proximity to the Sun. They integrated the trajectories using three different models of the Galactic potential: a local potential model, a global potential model and a perturbative potential model. The agreement between their models was generally good.

We are interested in knowing the approximate distance to the stars, where the straight line and local approximations differ significantly from the global model. To do so, we use the data of table 2 of García-Sánchez et al. (1999) for the closest encounters, using a simple rectilinear motion of the stars, and also the data for the closest encounters using a local Galactic potential.

In Table 3, we show 142 stars close to the Sun (within approximately 190 pc). From this sample, we obtain 74 ($\sim$52 per cent) stars for which the difference among the approximations to the potential employed (global, local or linear) is negligible. In Fig. 5, we show the relative errors of the closest approaches (missing distance errors), between the global versus straight-line approximations (blue triangles) and between the global versus local approximations (red squares), as a function of the distance from the Sun. From this figure, we can appreciate that the three approximations give the same results up to distances of $\sim$20 pc. Even for times as short as 10 Myr, stars beyond $\sim$20 pc have significant differences in their trajectories for the different approximations, showing where the Galactic global potential becomes important. A local potential clearly does better

Table 1. Astronomical data for the 34 stellar subsample run towards the past.

Star name	Parallax (arcsec)	PM(α) (arcsec yr^{-1})	PM(δ) (arcsec yr^{-1})	V_r (km s^{-1})	Miss distance (pc)	Time (10^3 yr)	$\mathrm{Vel_{App}}$ (km s^{-1})
GJ 65B (LHS10)	0.3737 ± 0.0060	3.3210 ± 0.0050	0.5620 ± 0.0050	29.0 ± 2.0	2.21 ± 0.07	-28.5 ± 0.9	51.64 ± 1.38
H16537 (GJ 144)	0.3108 ± 0.0009	-0.9764 ± 0.0010	0.0180 ± 0.0009	15.5 ± 0.9	2.23 ± 0.08	-105.5 ± 0.4	21.50 ± 0.73
H5643 (GJ 54.1)	0.2691 ± 0.0076	1.2101 ± 0.0052	0.6470 ± 0.0039	28.0 ± 5.0	2.43 ± 0.31	$-74.4^{+3.7}_{-0.6}$	36.99 ± 4.22
H24186 (GJ 191)	0.2553 ± 0.0009	6.5061 ± 0.0010	-5.7314 ± 0.0009	245.5 ± 2.0	2.15 ± 0.02	-10.9 ± 0.1	293.58 ± 1.90
H30920 (GJ 234A)	0.2429 ± 0.0026	0.6947 ± 0.0030	-0.6186 ± 0.0025	24.0 ± 5.0	2.48 ± 0.38	$-106.7^{+8.4}_{-2.8}$	30.09 ± 4.41
H103039 (LP816-60)	0.1820 ± 0.0037	-0.3067 ± 0.0038	0.0308 ± 0.0041	15.8 ± 0.6	2.49 ± 0.14	-270.2 ± 7.8	17.72 ± 0.61
H33226 (GJ 251)	0.1813 ± 0.0019	-0.7293 ± 0.0021	-0.3993 ± 0.0013	36.0 ± 10.0	2.85 ± 0.71	$-109.8^{+15.7}_{-8.8}$	42.06 ± 9.35
H40501 (GJ 2066)	0.1090 ± 0.0018	-0.3750 ± 0.0022	0.0601 ± 0.0015	62.2 ± 0.1	2.35 ± 0.08	-134.7 ± 2.1	64.36 ± 0.13
H14754 (HD20523)	0.0985 ± 0.0015	0.0419 ± 0.0015	-0.1041 ± 0.0019	65.9 ± 0.1	0.83 ± 0.03	-149.6 ± 2.4	66.12 ± 0.11
H22738 (GJ 2036A)	0.0890 ± 0.0036	0.1329 ± 0.0043	0.0739 ± 0.0038	40.1 ± 10.0	2.22 ± 0.90	$-263.2^{+52.4}_{-112.5}$	40.92 ± 10.95
H26335 (GJ 208)	0.0879 ± 0.0013	-0.0026 ± 0.0013	-0.0576 ± 0.0009	22.7 ± 5.0	1.55 ± 0.52	$-481.1^{+90.0}_{-188.3}$	22.91 ± 5.56
H95326 (CCDMJ19236)	0.0780 ± 0.0579	0.1017 ± 0.0749	-0.0216 ± 0.0417	35.6 ± 0.4	2.24 ± 26.40^{a}	$-341.3^{+123.5}_{-299.0}$	$36.16^{+22.22}_{-0.62}$
H27887 (GJ 2046)	0.0780 ± 0.0005	-0.0518 ± 0.0006	-0.0604 ± 0.0006	30.4 ± 0.2	2.02 ± 0.04	-402.1 ± 3.9	30.79 ± 0.22
H8709 (GJ 3121)	0.0630 ± 0.0038	0.0012 ± 0.0043	0.1241 ± 0.0024	64.0 ± 3.0	2.29 ± 0.33	-237.4 ± 19.5	64.68 ± 3.34
H12351 (GJ 1049)	0.0610 ± 0.0013	-0.0190 ± 0.0013	0.0303 ± 0.0013	26.2 ± 10.0	1.74 ± 3.16^{a}	$-604.5^{+188.0}_{-640.4}$	26.37 ± 10.96
GJ 54.2B (HD7438)	0.0574 ± 0.0009	0.1320 ± 0.0022	0.2830 ± 0.0021	16.0 ± 5.0	14.80 ± 1.38	$-296.5^{+78.7}_{-24.5}$	$30.36^{+3.53}_{-2.23}$
H32362 (GJ 242)	0.0570 ± 0.0008	-0.1152 ± 0.0007	-0.1909 ± 0.0005	211.1 ± 0.9	1.54 ± 0.05	-80.6 ± 1.2	211.91 ± 1.01
GJ 401B (LHS290)	0.0569 ± 0.0252	-1.8660 ± 0.0249	-0.6610 ± 0.0184	40.2 ± 6.5	$17.08^{+251.76}_{-5.07}$	-24.0 ± 10.4	$169.76^{+2511.15}_{-43.50}$
H27288 (GJ 217.1)	0.0460 ± 0.0007	-0.0148 ± 0.0006	-0.0012 ± 0.0005	25.6 ± 5.0	1.31 ± 0.38	$-827.1^{+142.6}_{-287.0}$	25.65 ± 5.61
H13772 (HD18455)	0.0445 ± 0.0026	0.0302 ± 0.0024	-0.0369 ± 0.0018	50.4 ± 0.2	2.25 ± 0.30	-431.4 ± 26.6	50.69 ± 0.23
H26373 (HD37572)	0.0419 ± 0.0017	0.0253 ± 0.0023	0.0000 ± 0.0022	32.4 ± 0.2	2.08 ± 0.25	-714.4 ± 31.1	32.55 ± 0.23
T100111 (HD351880)	0.0400 ± 0.0327	-0.0100 ± 0.0340	0.0074 ± 0.0270	26.1 ± 0.3	1.40 ± 70.48^{a}	$-933.4^{+370.5}_{-1163.6}$	$26.15^{+20.85}_{-0.34}$
H13769 (GJ 120.1C)	0.0389 ± 0.0015	0.0154 ± 0.0015	-0.0325 ± 0.0012	49.6 ± 0.5	2.26 ± 0.21	-502.6 ± 21.2	49.83 ± 0.56
H93506 (HD176687)	0.0370 ± 0.0014	-0.0141 ± 0.0026	0.0037 ± 0.0020	22.0 ± 5.0	2.25 ± 0.91	$-1192.9^{+231.3}_{-545.0}$	22.08 ± 5.60
H30067 (HD43947)	0.0360 ± 0.0009	-0.0175 ± 0.0010	-0.0143 ± 0.0007	40.5 ± 2.0	2.04 ± 0.19	-667.1 ± 41.7	40.60 ± 2.24
S14576 (ALGOL)	0.0350 ± 0.0009	0.0024 ± 0.0008	-0.0014 ± 0.0009	4.0 ± 0.9	2.54 ± 1.86^{a}	$-6893.3^{+1315.1}_{-2911.5}$	4.05 ± 1.00
H30344 (HD44821)	0.0340 ± 0.0008	-0.0030 ± 0.0005	0.0041 ± 0.0006	14.4 ± 0.2	1.44 ± 0.17	-1990.0 ± 59.0	14.44 ± 0.23
H54806 (HD97578)	0.0310 ± 0.0141	-0.0117 ± 0.0095	0.0018 ± 0.0099	23.5 ± 1.0	2.48 ± 15.52^{a}	$-1333.5^{+371.4}_{-1355.2}$	$23.59^{+1.64}_{-1.10}$
H31626 (HD260564)	0.0290 ± 0.0021	0.0095 ± 0.0018	-0.0332 ± 0.0013	82.7 ± 5.0	2.35 ± 0.44	$-405.8^{+35.4}_{-50.0}$	82.89 ± 5.61
H26624 (HD37594)	0.0240 ± 0.0007	-0.0039 ± 0.0006	0.0021 ± 0.0004	22.4 ± 1.3	1.67 ± 0.27	-1815.0 ± 134.9	22.43 ± 1.46
T31821 (HD47787)	0.0210 ± 0.0021	-0.0343 ± 0.0017	0.0274 ± 0.0025	18.3 ± 0.6	22.66 ± 4.65	-1966.5 ± 128.1	20.84 ± 0.82
H99483 (HIP99483)	0.0130 ± 0.0067	0.0013 ± 0.0214	0.0003 ± 0.0251	25.0 ± 0.2	1.95 ± 129.44^{a}	-3001.3 ± 1154.8	$25.07^{+13.47}_{-0.18}$
H40317 (HD68814)	0.0120 ± 0.0016	-0.0007 ± 0.0014	0.0020 ± 0.0012	34.2 ± 0.2	2.02 ± 2.15^{a}	$-2378.2^{+275.3}_{-428.3}$	34.27 ± 0.27
H101573 (HIP101573)	0.0050 ± 0.0023	-0.0002 ± 0.0024	0.0004 ± 0.0022	43.7 ± 0.5	2.55 ± 21.96^{a}	-4443.3 ± 1418.0	$44.15^{+0.91}_{-0.59}$

[a] The uncertainty value marked here corresponds to the radius of a cylinder where the locus of the closest approach is likely to lie.

than the straight-line approximation. For completeness, we compare the results of our global model including arms and bar, with the simple global model of García-Sánchez et al. (2001), which includes spiral arms. In this case, we find 73 per cent of our trajectories differ by less than 3 per cent, and for the rest (the most distant stars in general) the error is 6–26 per cent. Differences among stellar orbits due to the use of different models for the Galactic field or the simple straight-line approximation, become more important the farer the star is, making even more uncertain approaches to the Sun in its path for the Milky Way disc. Deeper and precise observations as the ones are coming in the near future, will improve dramatically our knowledge on this field, and will make more important to use better models of the Galaxy.

3.1.4 The Solar system under the influence of stellar encounters at the solar neighbourhood

The overarching goal of our work in this set of papers will be to address quantitatively the effect of stellar encounters on different Galactic environments. In this section, we start with the nascent Solar system and the current stellar environment. For this purpose, we model a simple planetary system (or disc) with 1000 particles distributed from 1 to 100 au. We study this system for a total integration time of 10 000 yr, which is much longer than the typical encounter time-scale.

We chose the parameters of Gliese 710 (0.6 $\mathrm{M}_{\odot}$, approximation velocity 13.9 km s^{-1}) and an estimated closest approach less than 0.3 pc, 1.4 Myr in the future, to calculate its effects on the Solar system. The effect of this specific star will be interesting for the Oort Cloud, but we find that Gliese 710's effect is negligible for a 100 au planetary system.

We ran a grid of simulations for a flyby star mass of 1 $\mathrm{M}_{\odot}$ and closest approaches between 100 and 1000 au, in steps of 50 au. Disc disruption starts to be significant for approaches within about 200 au. We also find a good agreement to the analytical result of Hall, Clarke & Pringle (1996) where they find that a disc is affected to $\sim$1/3 the closest approach distance. With these parameters and the velocity of GJ 710 (13.9 km s^{-1}), we calculate the gravitational effect on a planetary disc and we present it in Fig. 6. The figure shows four panels, representing the orbits of particles in x–y (left frames) and x–z (right frames) planes, before (upper frames) and after (lower frames). Fig. 7 shows the resultant orbital characteristics of the disc after the encounter, eccentricity of particles (upper left

Table 2. Astronomical data for the 33 stellar subsample run towards the future.

Star name	Parallax (arcsec)	PM (α) (arcsec yr^{-1})	PM (δ) (arcsec yr^{-1})	V_r (km s^{-1})	Miss distance (pc)	Time (10^3 yr)	$\mathrm{Vel_{App}}$ (km s^{-1})
H70890 (Proxima)	0.7723 ± 0.0024	-3.7756 ± 0.0015	0.7682 ± 0.0018	-21.7 ± 0.5	0.95 ± 0.01	26.7 ± 0.1	32.10 ± 0.39
H71683 (AlphCenA)	0.7421 ± 0.0014	-3.6200 ± 0.0015	0.7100 ± 0.0012	-20.7 ± 0.9	1.01 ± 0.02	$27.7^{+0.1}_{-0.2}$	31.37 ± 0.67
H71681 (AlphCenB)	0.7421 ± 0.0014	-3.6004 ± 0.0261	0.9521 ± 0.0198	-24.6 ± 0.9	0.94 ± 0.02	27.7 ± 0.2	34.22 ± 0.74
H87937 (Barnard)	0.5490 ± 0.0016	-0.7978 ± 0.0016	10.3269 ± 0.0013	-106.8 ± 0.2	1.17 ± 0.01	9.8 ± 0.1	139.30 ± 0.25
H54035 (GJ 411)	0.3924 ± 0.0009	-0.5802 ± 0.0008	-4.7671 ± 0.0008	-85.0 ± 0.9	1.44 ± 0.01	20.0 ± 0.1	102.91 ± 0.84
S32349 (Sirius)	0.3792 ± 0.0016	-0.5460 ± 0.0013	-1.2231 ± 0.0012	-9.4 ± 0.9	2.30 ± 0.06	$65.8^{+3.0}_{-4.5}$	19.20 ± 0.50
H92403 (GJ 729)	0.3365 ± 0.0018	0.6376 ± 0.0022	-0.1925 ± 0.0015	-4.0 ± 2.0	2.73 ± 0.22	$111.8^{+24.6}_{-57.9}$	$10.20^{+1.12}_{-0.55}$
GJ 905 (LHS549)	0.3160 ± 0.0020	0.0850 ± 0.0050	-1.6150 ± 0.0050	-81.0 ± 5.0	0.91 ± 0.06	35.1 ± 2.1	84.56 ± 5.39
H57548 (GJ 447)	0.2996 ± 0.0022	0.6056 ± 0.0021	-1.2192 ± 0.0019	-31.0 ± 0.2	1.91 ± 0.03	71.0 ± 0.3	37.75 ± 0.21
GJ 866A (LHS68)	0.2895 ± 0.0050	2.3640 ± 0.0050	2.2360 ± 0.0050	-60.0 ± 2.0	2.29 ± 0.08	$31.5^{+0.1}_{-0.2}$	80.24 ± 1.82
H104214 (GJ 820A)	0.2871 ± 0.0015	4.1551 ± 0.0010	3.2589 ± 0.0012	-64.3 ± 0.9	2.80 ± 0.03	18.7 ± 0.1	108.34 ± 0.73
H110893 (GJ 860A)	0.2495 ± 0.0030	-0.8702 ± 0.0030	-0.4711 ± 0.0030	-24.0 ± 5.0	2.47 ± 0.36	$101.2^{+2.2}_{-7.2}$	30.49 ± 4.37
H85605 (CCDMJ)	0.2027 ± 0.0395	0.0973 ± 0.0267	0.3489 ± 0.0413	-21.1 ± 0.2	$1.84^{+1.20}_{-0.47}$	$197.0^{+36.5}_{-25.4}$	$22.74^{+1.18}_{-0.52}$
H86214 (GJ 682)	0.1983 ± 0.0024	-0.7101 ± 0.0028	-0.9380 ± 0.0021	-60.0 ± 10.0	2.14 ± 0.36	67.4 ± 7.8	66.27 ± 10.12
H97649 (GJ 768)	0.1944 ± 0.0009	0.5368 ± 0.0007	0.3855 ± 0.0007	-26.1 ± 0.9	2.70 ± 0.08	139.5 ± 2.4	30.68 ± 0.86
H57544 (GJ 445)	0.1855 ± 0.0014	0.7432 ± 0.0016	0.4804 ± 0.0012	-119.0 ± 5.0	1.01 ± 0.05	43.0 ± 1.9	121.13 ± 5.53
H86990 (GJ 693)	0.1721 ± 0.0022	-1.1199 ± 0.0021	-1.3525 ± 0.0015	-115.0 ± 21.0	2.25 ± 0.44	$42.0^{+7.0}_{-4.9}$	124.76 ± 21.61
H99461 (GJ 783A)	0.1652 ± 0.0009	0.4569 ± 0.0009	-1.5749 ± 0.0006	-129.8 ± 0.9	2.06 ± 0.03	40.3 ± 0.3	138.07 ± 0.96
H86961 (GJ 2130A)	0.1618 ± 0.0113	-0.0498 ± 0.0929	-0.3198 ± 0.0473	-28.9 ± 0.9	1.93 ± 0.41	188.8 ± 12.4	30.42 ± 1.09
H86963 (GJ 2130B)	0.1618 ± 0.0113	-0.0776 ± 0.0136	-0.2701 ± 0.0078	-27.4 ± 0.9	1.78 ± 0.28	202.3 ± 13.7	28.61 ± 0.97
H83945 (GJ 3991)	0.1378 ± 0.0090	0.3339 ± 0.0081	-0.2780 ± 0.0103	-45.0 ± 10.0	2.29 ± 0.71	$142.0^{+37.8}_{-22.1}$	47.42 ± 10.58
H93449 (RCrA)	0.1218 ± 0.0682	-0.0344 ± 0.0975	0.0506 ± 0.0520	-36.0 ± 5.0	0.54 ± 27.21^{a}	$222.0^{+462.7}_{-76.4}$	$36.08^{+14.33}_{-5.55}$
H77257 (GJ 598)	0.0851 ± 0.0008	-0.2255 ± 0.0008	-0.0685 ± 0.0007	-66.4 ± 0.9	2.28 ± 0.06	166.5 ± 2.8	67.69 ± 1.00
H116727 (GJ 903)	0.0725 ± 0.0005	-0.0489 ± 0.0005	0.1272 ± 0.0004	-42.4 ± 0.9	2.84 ± 0.08	305.0 ± 6.9	43.33 ± 0.99
H6379 (GJ 56.5)	0.0595 ± 0.0006	-0.0341 ± 0.0005	-0.0345 ± 0.0006	-22.7 ± 2.0	2.82 ± 0.29	$703.4^{+79.7}_{-55.7}$	23.03 ± 2.22
H89825 (GJ 710)	0.0518 ± 0.0014	0.0017 ± 0.0014	0.0021 ± 0.0011	-13.9 ± 2.0	0.34 ± 0.28^{a}	$1357.8^{+312.1}_{-172.7}$	13.90 ± 2.25
H113421 (HD217107)	0.0507 ± 0.0008	-0.0061 ± 0.0008	-0.0160 ± 0.0006	-14.0 ± 0.6	2.22 ± 0.16	1355.5 ± 67.0	14.16 ± 0.67
H38228 (HD63433)	0.0458 ± 0.0009	-0.0093 ± 0.0010	-0.0118 ± 0.0007	-16.5 ± 0.2	2.08 ± 0.16	1281.6 ± 31.0	16.58 ± 0.22
H105766 (GJ 4194)	0.0389 ± 0.0006	0.0412 ± 0.0006	0.0396 ± 0.0006	-76.9 ± 0.2	2.32 ± 0.07	324.2 ± 5.3	77.22 ± 0.23
H20359 (GJ 168)	0.0326 ± 0.0020	-0.0348 ± 0.0018	0.0111 ± 0.0015	-78.5 ± 5.0	2.07 ± 0.34	380.3 ± 37.0	78.68 ± 5.61
H21386 (HD26367)	0.0273 ± 0.0015	0.0135 ± 0.0013	0.0090 ± 0.0017	-50.7 ± 2.0	2.01 ± 0.29	704.1 ± 51.3	50.80 ± 2.25
H85661 (HD158576)	0.0115 ± 0.0008	0.0010 ± 0.0009	0.0000 ± 0.0004	-46.0 ± 1.7	0.97 ± 0.89^{a}	1847.7 ± 157.1	46.02 ± 1.89
H94512 (HD1779939)	0.0085 ± 0.0009	-0.0001 ± 0.0007	-0.0005 ± 0.0005	-30.1 ± 2.0	1.49 ± 1.95^{a}	3821.3 ± 480.8	30.10 ± 2.20

[a] The uncertainty value marked here corresponds to the radius of a cylinder where the locus of the closest approach is likely to lie.

frame), inclination (upper right frame), pericentre distance (lower-left frame) and apocentre distance (lower right frame), all plotted versus the semimajor axis. The effect on the disc is slight but clear starting at 40 au, where particles reach an eccentricity up to 0.1.

3.1.5 Effect of Gliese 710 on the Oort Cloud

The Solar system's disc and Kuiper belt are surrounded by the Oort Cloud, which contains 1×10^{11}–5×10^{12} cometary nuclei with a total mass $\sim$1–50 $\mathrm{M}_{\oplus}$ (Stern 2003). Comets in the Oort Cloud evolve dynamically under the influence of external perturbers such as random stellar passages. Close or penetrating passages of stars through the Oort Cloud can deflect comets towards the inner planetary region (Hills 1981; Weissman 1996; Brasser, Duncan & Levison 2006, 2007, 2008; Kirsh et al. 2009).

One important issue in the scenario of the flyby star is the effect it would have on the loosely bound outer Oort Cloud. Small gravitational perturbations could have severe effects on the cloud due to the direct effect on the Sun. A simple calculation using the impulse approximation predicts that during the stellar encounter the velocity of the Sun would change by $\delta_{\mathrm{v}} \approx \frac{2\,GM_{\star}}{q_{\star}\,v_{\infty}}$. With the values of Gliese 710, for the stellar mass $M_{\star} = 0.6\,\mathrm{M}_{\odot}$, the closest distance of the encounter, $q_{\star} = 0.34$ pc ($\sim$70 000 au) and the velocity at infinity, $v_{\infty} = 13.4\,\mathrm{km\,s^{-1}}$. This would result in $5.8 \times 10^{-4}\,\mathrm{km\,s^{-1}}$ change in the solar velocity, a negligible value compared with the typical Oort Cloud speed of $0.2\,\mathrm{km\,s^{-1}}$ or with its escape velocity at the boundary ($\sim$$0.1\,\mathrm{km\,s^{-1}}$), so Gliese 710 has no ability to strip the Oort Cloud from the Sun. However, it has the potential to send a comet flux towards the inner Solar system. This will cause the appearance of a new comet every year and the net increase of the risk of astronomic impact will not be detectable (García-Sánchez et al. 2001).

4 SECOND GALACTIC REGION: THE BIRTH CLOUD OF THE SUN

In star formation regions such as the Sun's putative birth location inside a dense cluster, stellar densities are high enough to produce stellar encounters within 300 au before the dissolution of the stellar cluster (Laughlin & Adams 1998; Adams 2010). Also, in this environment, encounters are stronger owing to lower typical velocity dispersions between 1 and $3\,\mathrm{km\,s^{-1}}$. Let us consider, for example, a planetary disc around a given star on a crowded stellar environment. Let us assume solar mass stars for generality. The star–disc system

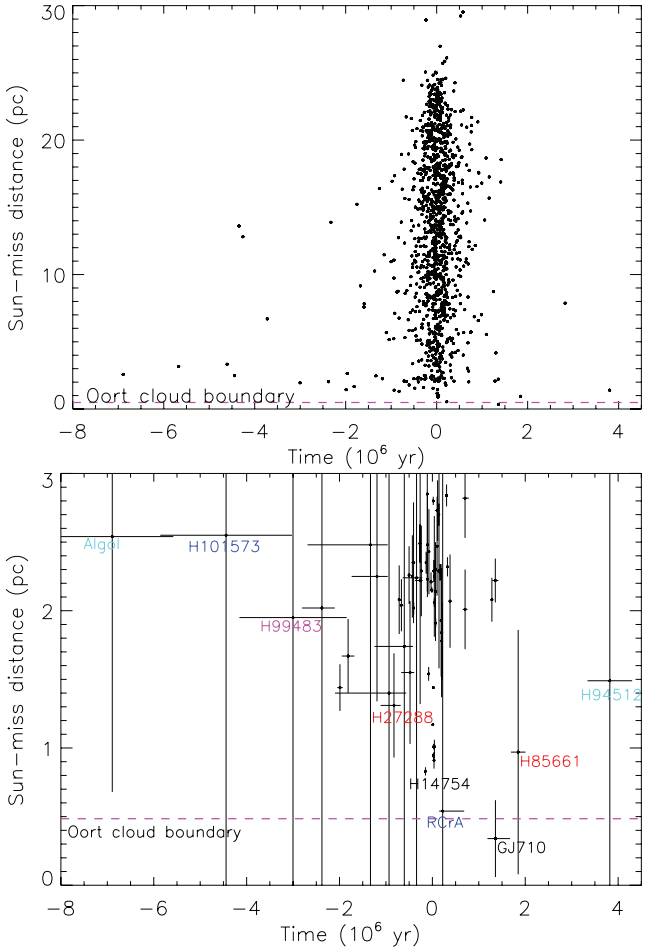

Figure 2. Miss distance versus time of stellar approaches for those stars in the total sample of 1167 stars within 30 pc as the maximum approach distance to the Sun. The Oort Cloud boundary at ∼0.48 pc is plotted as reference. The lower frame is a zoom that shows a subsample with the closest approach distances (less than 3 pc) to the Sun (see Tables 1 and 2) and their computed uncertainties. Some stars' names are illustrated in the figure.

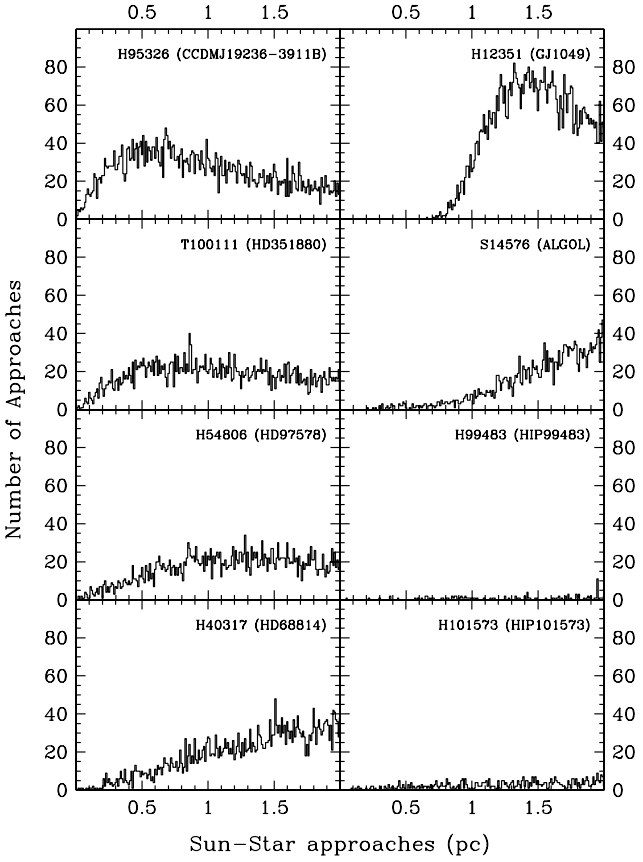

Figure 3. Histograms computed on eight stars from our sample to the past with large enough observational error bars that may produce approach distances between the Sun and the star below zero. All plots show the Sun–star approaches in parsec from a set of 10 000 normal deviation random initial conditions within the observational error bars.

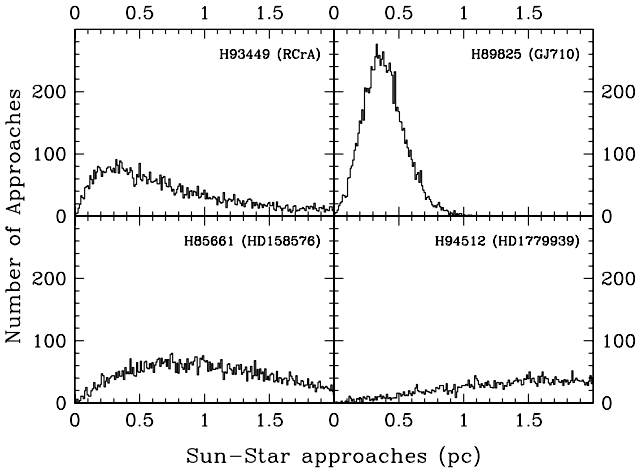

Figure 4. Same as Fig. 3 but for four stars to the future.

will experience encounters with other systems with an interaction rate that can be written as $\gamma = \langle n\sigma v\rangle = \langle n\rangle\langle\sigma\rangle\langle v\rangle$, where n is the number density of stars in the cluster, σ is the cross-section of interaction and v is the relative velocity (velocity dispersion in this case). For a rough estimate of the interaction rate among stars, we use the typical values for open clusters. In their work, Laughlin & Adams (1998) calculate the interaction rate for the Trapezium cluster, using a central density of $n_0 \approx 5 \times 10^4$ pc^{-3} and a velocity dispersion of a few km s^{-1}, and an interaction cross-section of 100^2 au^2, obtaining a rate of interaction of one encounter every 40 Myr. Considering open clusters live for at least 100 Myr, it is expected that these interactions are significant in those environments. In the case of the Sun's birth cloud several observables, such as the inclinations of Uranus and Neptune (which are sensitive to stellar interactions), place densities at similar amounts of typical open clusters, that is, $\sim 3 \times 10^4$ M$_\odot$ pc^3 (Gaidos 1995). Furthermore, the orbit of (90377) Sedna supports the idea that the Solar system was born in a stellar cluster with a non-negligible density (Kenyon & Bromley 2004; Morbidelli & Levison 2004; Brasser et al. 2006).

In this section, we present experiments to reproduce some of the Kuiper belt bodies' orbital characteristics, such as eccentricities and inclinations. We have chosen four close-approach distances (200, 150, 100 and 50 au), coupled with three initial approach velocities (1, 2 and 3 km s^{-1}) for a stellar flyby interacting with a 100 au disc of particles. The mass of the perturbing star is 1 M$_\odot$, and angles involved in the geometry of stellar encounter have the general values, $\theta = 45^\circ$ (the angle between the plane of the stellar

Table 3. Relative errors between different approximations to the Galactic potential. Column 1 is the name of the object. Columns 2, 3 and 4 show the close-approach distance to the Sun in pc with the global (from this work), local and straight-line approximations (García-Sánchez et al. 1999, 2001); Columns 5, 6 and 7 present the relative errors (G=global, Lo=local, Li=Linear) and the last column is the current distance to the star in parsec.

Star name	Global	Local Missing distance (pc)	Linear	(G-Lo)/G	(G-Li)/G (per cent)	(Lo-Li)/Lo	Distance (pc)
GJ 710	0.337	0.336	0.343	0.3	1.8	2.1	19.30
HD 158576	0.938	0.846	0.753	9.8	19.7	11.0	86.81
Proxima	0.954	0.954	0.954	0.0	0.0	0.0	1.29
Alpha Centauri A	0.973	0.973	0.973	0.0	0.0	0.0	1.35
Alpha Centurai B	0.975	0.975	0.975	0.0	0.0	0.0	1.35
AC + 79 3888	1.007	1.007	1.007	0.0	0.0	0.0	5.39
GJ 620.1B	4.259	1.139	1.139	73.3	73.3	0.0	12.81
Barnard Star	1.144	1.143	1.143	0.1	0.1	0.0	1.82
HD 351880	1.434	1.439	1.445	0.3	0.8	0.4	25.27
Lalande 21185	1.440	1.440	1.440	0.0	0.0	0.0	2.55
SAO 75395	2.469	1.448	2.688	41.4	8.9	85.6	118.34
HD 179939	1.444	1.451	1.025	0.5	29.0	29.4	117.10
GJ 208	1.600	1.600	1.599	0.0	0.1	0.1	11.38
HD 37594	1.637	1.610	1.598	1.6	2.4	0.7	41.39
GJ 217.1	1.645	1.637	1.629	0.5	1.0	0.5	21.52
HIP 99483	1.797	1.653	1.379	8.0	23.3	16.6	74.13
HD 35317	1.775	1.755	1.735	1.1	2.3	1.1	58.04
GJ 2130 B	1.782	1.782	1.782	0.0	0.0	0.0	6.18
HD 19995	1.254	1.811	2.653	44.4	111.6	46.5	68.54
HIP 101573	2.072	1.821	1.898	12.1	8.4	4.2	187.62
CCDM 17296 + 2439 B	1.837	1.837	1.837	0.0	0.0	0.0	4.93
GJ 358	1.875	1.875	1.875	0.0	0.0	0.0	9.49
ROSS 154	1.881	1.881	1.881	0.0	0.0	0.0	2.97
HD 68814	1.950	1.909	1.990	2.1	2.1	4.2	82.10
ROSS 128	1.911	1.911	1.911	0.0	0.0	0.0	3.34
GJ 2130 A	1.929	1.929	1.929	0.0	0.0	0.0	6.18
GJ 860 A	1.949	1.949	1.949	0.0	0.0	0.0	4.01
HD 33487	2.001	1.977	1.954	1.2	2.3	1.2	41.63
HD 43947	2.015	2.016	2.016	0.0	0.0	0.0	27.53
HD 26367	2.019	2.028	2.038	0.4	0.9	0.5	36.66
GJ 271 A	2.044	2.038	2.029	0.3	0.7	0.4	18.03
GJ 168	2.074	2.074	2.075	0.0	0.0	0.0	30.69
GJ 144	2.135	2.135	2.135	0.0	0.0	0.0	3.22
HD 63433	2.150	2.138	2.121	0.6	1.3	0.8	21.82
GJ 682	2.140	2.140	2.140	0.0	0.0	0.0	5.04
GJ 120.1	2.243	2.245	2.246	0.1	0.1	0.0	22.48
GJ 693	2.253	2.253	2.253	0.0	0.0	0.0	5.81
CCDM 19236 − 3911 B	2.262	2.261	2.260	0.0	0.1	0.0	12.87
HD 122676	2.264	2.263	2.262	0.0	0.1	0.0	26.12
GJ 598	2.267	2.267	2.267	0.0	0.0	0.0	11.75
GJ 120.1 C	2.267	2.269	2.269	0.1	0.1	0.0	25.73
WD 0148+467	2.286	2.286	2.286	0.0	0.0	0.0	15.85
SIRIUS	2.299	2.299	2.299	0.0	0.0	0.0	2.64
HD 37574	2.290	2.305	2.233	0.7	2.5	3.1	62.00
HD 217107	2.300	2.313	2.323	0.6	1.0	0.4	19.72
HD 176687	2.299	2.314	2.333	0.7	1.5	0.8	27.31
BD -02 3986	1.804	2.316	3.102	28.4	72.0	33.9	58.48
HD 67852	2.932	2.341	1.229	20.2	58.1	47.5	118.34
HD 260564	2.341	2.341	2.340	0.0	0.0	0.0	34.42
ALGOL	2.481	2.381	2.666	4.0	7.5	12.0	28.46
GJ 54.1	2.429	2.429	2.429	0.0	0.0	0.0	3.72
LP 816 − 60	2.482	2.482	2.483	0.0	0.0	0.0	5.49
HD 50867	2.540	2.587	2.732	1.9	7.6	5.6	51.47
GJ 16	2.596	2.609	2.623	0.5	1.0	0.5	16.22
HD 34790	2.477	2.647	2.862	6.9	15.5	8.1	85.32
IRAS 17249+0416	2.670	2.664	2.658	0.2	0.4	0.2	50.08
HD 152912	2.860	2.700	2.466	5.6	13.8	8.7	139.28
GJ 768	2.702	2.702	2.702	0.0	0.0	0.0	5.14
GJ 903	2.791	2.791	2.792	0.0	0.0	0.0	13.79

Table 3 – *continued*

Star name	Global	Local Missing distance (pc)	Linear	(G-Lo)/G	(G-Li)/G (per cent)	(Lo-Li)/Lo	Distance (pc)
HD 172748	2.801	2.806	2.823	0.2	0.8	0.6	57.34
GJ 56.5	2.825	2.823	2.823	0.1	0.1	0.0	16.82
GJ 908	2.886	2.886	2.885	0.0	0.0	0.0	5.97
HD 221420	2.917	2.907	2.886	0.3	1.1	0.7	31.76
HD 142500	3.247	2.917	2.458	10.2	24.3	15.7	73.86
ROSS 614	2.929	2.929	2.929	0.0	0.0	0.0	4.12
GJ 1095	2.969	2.969	2.968	0.0	0.0	0.0	16.86
ROSS 882	3.053	3.052	3.052	0.0	0.0	0.0	5.93
HD 148317	3.268	3.132	2.903	4.2	11.2	7.3	79.87
HD 150689	3.145	3.145	3.146	0.0	0.0	0.0	14.37
GJ 169	3.189	3.189	3.188	0.0	0.0	0.0	11.47
GJ 279	3.196	3.196	3.197	0.0	0.0	0.0	25.70
GJ 628	3.208	3.208	3.208	0.0	0.0	0.0	4.26
GJ 687	3.213	3.213	3.213	0.0	0.0	0.0	4.53
GJ 231	3.249	3.249	3.249	0.0	0.0	0.0	10.15
HD 38382	3.271	3.271	3.273	0.0	0.1	0.1	25.54
GJ 71	3.271	3.271	3.271	0.0	0.0	0.0	3.65
GJ 1005	3.289	3.289	3.289	0.0	0.0	0.0	5.21
Van Maanen'a star	3.327	3.327	3.327	0.0	0.0	0.0	4.41
HD 28676	3.681	3.380	2.966	8.2	19.4	12.2	39.14
GJ 722	3.384	3.384	3.384	0.0	0.0	0.0	12.98
HD 233081	3.412	3.396	3.355	0.5	1.7	1.2	51.02
GJ 280 A	3.438	3.438	3.438	0.0	0.0	0.0	3.50
GJ 15A	3.467	3.469	3.469	0.1	0.1	0.0	3.57
GJ 678	3.503	3.503	3.503	0.0	0.0	0.0	16.45
GJ 725 B	3.515	3.515	3.515	0.0	0.0	0.0	3.52
HD 199881	4.355	3.527	3.106	19.0	28.7	11.9	80.45
HD 67523	3.563	3.563	3.564	0.0	0.0	0.0	19.23
GJ 725A	3.568	3.568	3.568	0.0	0.0	0.0	3.57
GJ 66	3.569	3.570	3.570	0.0	0.0	0.0	8.15
HD 168769	3.540	3.594	3.662	1.5	3.4	1.9	50.33
Luyten star	3.666	3.666	3.666	0.0	0.0	0.0	3.80
GJ 825	3.696	3.696	3.696	0.0	0.0	0.0	3.95
GJ 784	3.727	3.727	3.727	0.0	0.0	0.0	6.20
GJ 775	3.756	3.756	3.756	0.0	0.0	0.0	13.11
GJ 96	3.756	3.756	3.756	0.0	0.0	0.0	11.91
GJ 251	3.813	3.814	3.814	0.0	0.0	0.0	5.52
BD + 37 4901C	3.940	3.820	3.622	3.0	8.1	5.2	33.80
GJ 380	3.856	3.856	3.856	0.0	0.0	0.0	4.87
GJ 252	3.869	3.867	3.862	0.1	0.2	0.1	17.27
HD 122064	3.868	3.868	3.868	0.0	0.0	0.0	10.10
HD 168956	4.134	3.940	3.762	4.7	9.0	4.5	73.69
HD 53253	3.527	3.998	4.381	13.4	24.2	9.6	125.16
HD 146214	4.394	4.034	4.007	8.2	8.8	0.7	93.63
GJ 791.1A	4.021	4.053	4.103	0.8	2.0	1.2	30.27
GJ 268	4.066	4.066	4.066	0.0	0.0	0.0	6.36
HD 192869	3.979	4.080	4.072	2.5	2.3	0.2	111.98
HD 33959C	4.092	4.093	4.097	0.0	0.1	0.1	25.14
GJ 337.1	4.117	4.121	4.121	0.1	0.1	0.0	19.56
GJ 674	4.134	4.134	4.134	0.0	0.0	0.0	4.54
GJ 620.1A	4.153	4.155	4.158	0.0	0.1	0.1	12.87
GJ 103	4.180	4.180	4.180	0.0	0.0	0.0	11.51
GJ 851	4.205	4.203	4.203	0.0	0.0	0.0	11.44
HD 170296	4.256	4.278	4.280	0.5	0.6	0.0	89.37
GJ 222	4.380	4.380	4.380	0.0	0.0	0.0	8.66
GJ 752A	4.420	4.420	4.420	0.0	0.0	0.0	5.87
HD 218200	4.856	4.429	4.062	8.8	16.4	8.3	74.91
HD 207164	2.720	4.449	7.785	63.6	186.2	75.0	75.87
GJ 688	4.461	4.461	4.460	0.0	0.0	0.0	10.71
HD 58954	4.467	4.483	4.343	0.4	2.8	3.1	85.98

Table 3 – *continued*

Star name	Global	Local Missing distance (pc)	Linear	(G-Lo)/G	(G-Li)/G (per cent)	(Lo-Li)/Lo	Distance (pc)
GJ 716	4.484	4.484	4.484	0.0	0.0	0.0	13.21
HD 32450	4.488	4.489	4.490	0.0	0.0	0.0	8.52
HD 162102	4.430	4.518	4.629	2.0	4.5	2.5	64.68
GJ 68	4.572	4.573	4.573	0.0	0.0	0.0	7.47
HD 71974	4.639	4.612	4.564	0.6	1.6	1.0	28.71
HD 163547	4.056	4.648	5.170	14.6	27.5	11.2	149.93
ROSS 780	4.690	4.690	4.690	0.0	0.0	0.0	4.70
GJ 702	4.698	4.698	4.698	0.0	0.0	0.0	5.09
GJ 178	4.701	4.701	4.701	0.0	0.0	0.0	8.03
GJ 701	4.720	4.720	4.720	0.0	0.0	0.0	7.80
HD 72617	4.760	4.762	4.748	0.0	0.3	0.3	58.07
GJ 832	4.828	4.828	4.828	0.0	0.0	0.0	4.94
GJ 638	4.834	4.834	4.834	0.0	0.0	0.0	9.77
GJ 713	4.838	4.838	4.838	0.0	0.0	0.0	8.06
HD 239927	4.862	4.871	4.890	0.2	0.6	0.4	57.44
GJ 625	4.896	4.896	4.896	0.0	0.0	0.0	6.58
HD 67228	4.924	4.924	4.925	0.0	0.0	0.0	23.33
GJ 735	4.926	4.927	4.927	0.0	0.0	0.0	11.59
HD 75935	4.857	4.938	5.063	1.7	4.2	2.5	40.55
GJ 410	4.973	4.976	4.980	0.1	0.1	0.1	11.66
HD 39655	4.694	4.979	5.197	6.1	10.7	4.4	102.77
GJ 644	4.982	4.982	4.982	0.0	0.0	0.0	5.74
HD 120702	4.820	4.993	5.184	3.6	7.6	3.8	96.25

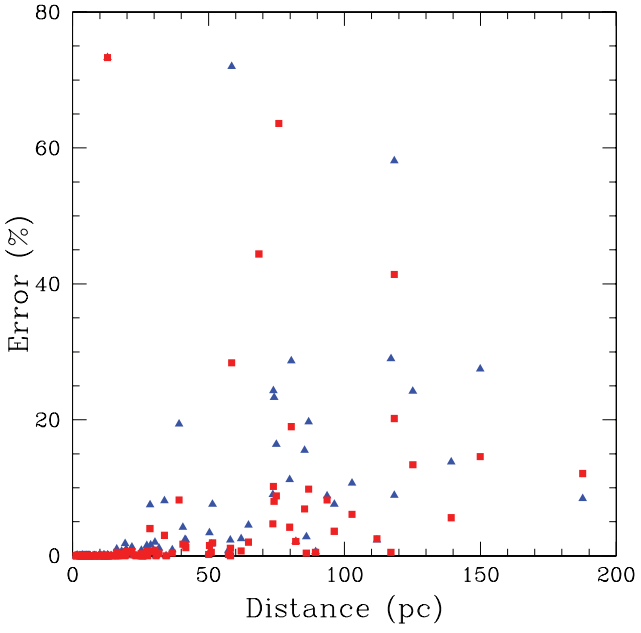

Figure 5. Relative error between the global and the straight-line approximations to the Galactic potential (blue triangles) and between the global and local approximations (red squares).

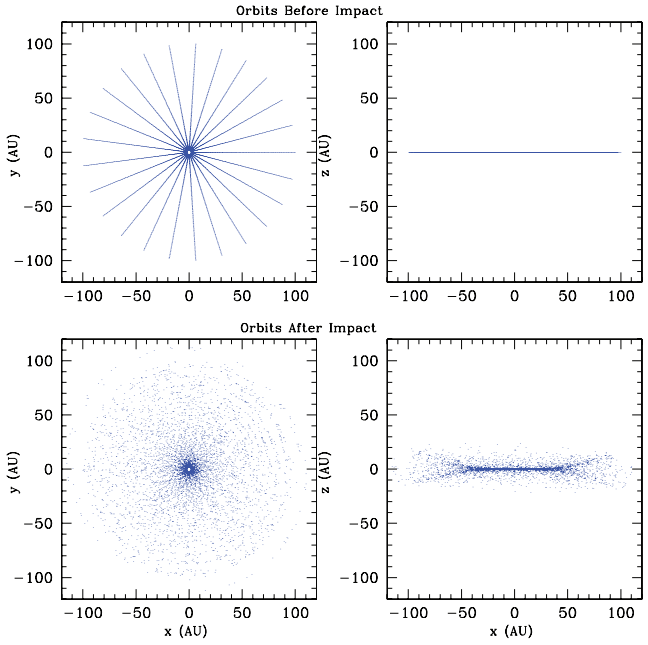

Figure 6. Effect of a stellar flyby mass of 1 $M_{\odot}$, closest approach of 300 au and velocity of 13.9 km s^{-1} on a disc of particles. Left frames: orbits of the particles in x–y cuts; right frames: cut in the x–z plane. Upper frames: particles before the encounter; lower frames: particles after the encounter.

trajectory and the plane of the disc) and $\alpha = 45^{\circ}$ (the angle between the axis of the stellar trajectory plane and the axis of the disc).

In our initial conditions, test particles have $e = i = 0$. In Fig. 8, we show our results of perturbations produced in the disc of particles by a flyby. The columns represent different values of the initial approach velocity (1, 2 and 3 km s^{-1}) and the rows represent different values of closest approach distances (50, 100, 150 and 200 au). Each panel shows the positions of the test particles in the x–z plane after the encounter with the flyby star.

In Figs 9 and 10 we show the resultant eccentricities and inclinations, plotted versus the semimajor axis. The columns represent different distances of the closest approach, within 200 au, and the rows

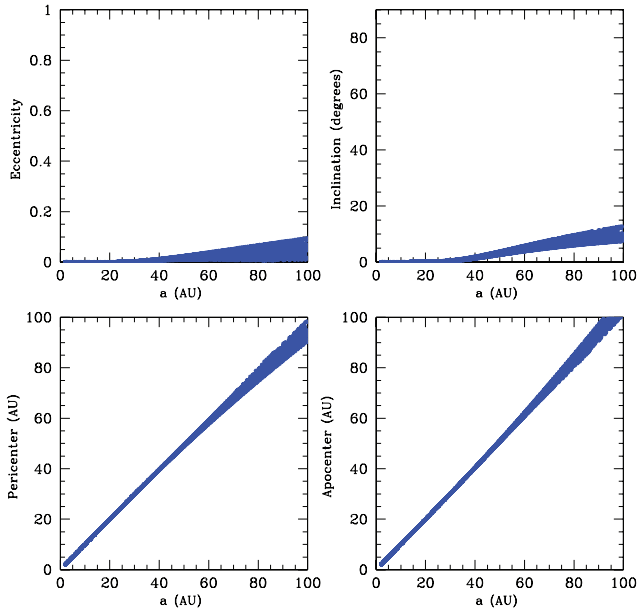

Figure 7. Resultant orbital characteristics on the disc of Fig. 6 after the encounter. Upper-left frame: eccentricity; upper-right frame: inclination; lower-left frame: pericentre distance and lower-right frame: apocentre distance. All versus the semimajor axis.

indicate different values of velocity dispersion, within 3 km s^{-1}. As a reference, in all plots, we include the known Kuiper belt objects, including the resonant and classic objects (pink triangles), and the scattered objects, including also Centaurs at radii less than 30 au (green crosses).

Our best fit occurs at a distance of the maximum approach between 100 and 150 au and at a velocity of $\sim$1 km s^{-1}, with an unaltered inner planetary system (as far as 30 au) where most of the particles between 30 and 50 au have eccentricities up to 0.2 and $i < 20^{\circ}$. In this simulation we also obtain some dispersed objects with high eccentricities and low semimajor axis as many of the objects seen in the planetary system. From 42 to approximately 48 au there are objects with eccentricities up to 0.4. We are able to match these objects using encounters with a velocity at infinity of 1 km s^{-1} and a close-approach distance of 100 au. This results in eccentricities from 0 to 0.1 on the semimajor axis in the interval of 0–40 au and eccentricities from 0 to 1 on the semimajor axis in the interval of 40–65 au and from 65 until 100 au, the most of particles are dynamically evaporated; this means that objects with low eccentricities and large semimajor axes (larger than 50 or 60 au) are scarce in these experiments as is the case in the Kuiper belt.

5 CONCLUSIONS

This paper is the first step in an extensive study of the gravitational effect of a flyby star on a 100 au disc, representing debris discs (and/or planetary systems) given the particular conditions of several environments of the Galaxy. In this work, we analysed the effect of the solar neighbourhood and the birth cloud of the Sun. In the current solar neighbourhood, we find that Gliese 710 will be the closest star to the Sun (1.36 Myr) in the future with a minimum distance of 0.34 pc ($\sim$70 000 au). This stellar encounter will lead to direct interactions between the star and the Oort Cloud. This star has a mass of 0.6 $M_{\odot}$ currently located at 19.3 pc from the Sun. We calculated its velocity at the point of minimum distance with the Sun as 14 km s^{-1}. The effect generated by Gliese 710 on a 100 au planetary system will be negligible. The minimum distance

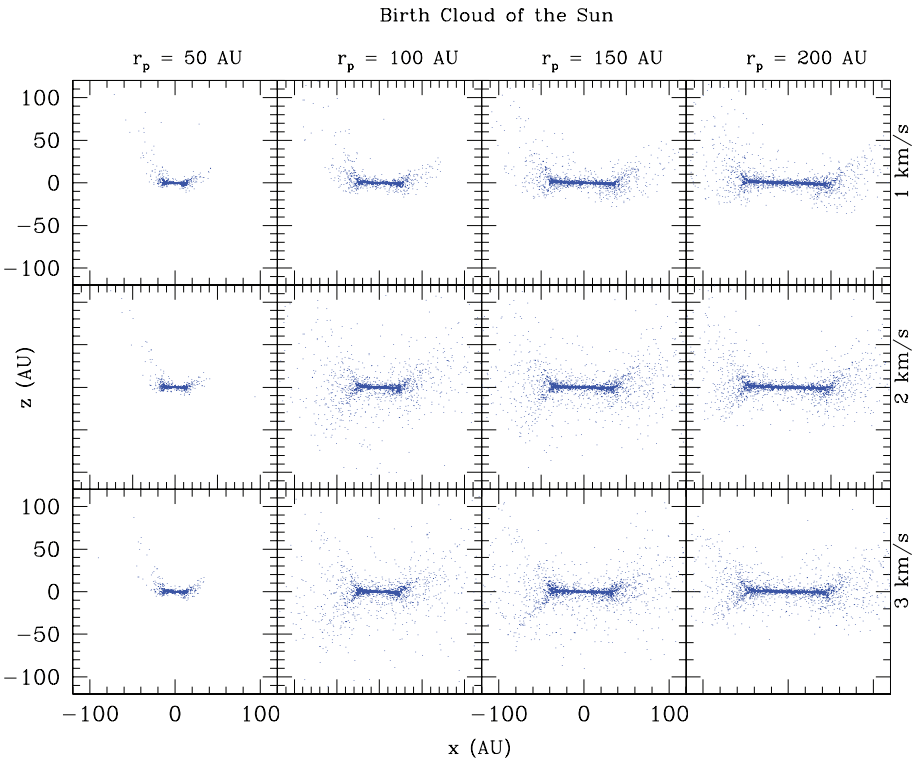

Figure 8. Final disc structure after a stellar encounter simulating a Galactic environment of star formation. Rows represent values of velocity dispersion within 3 km s^{-1} and columns represent different impact parameters within 200 au

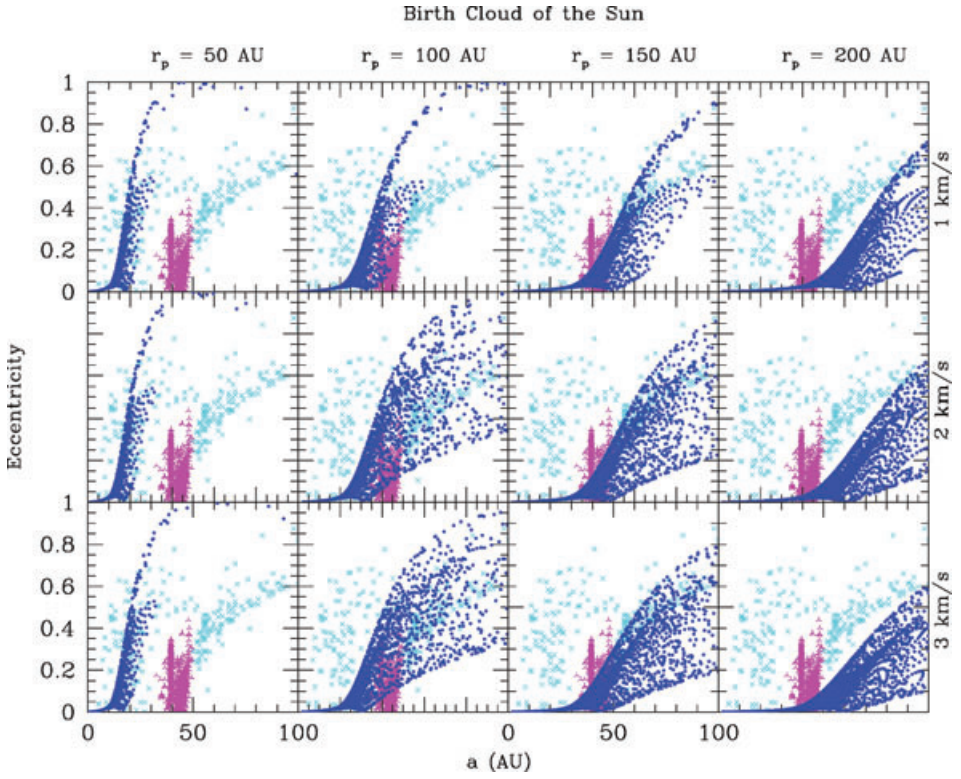

Figure 9. Resultant eccentricities. Rows indicate different values of velocity dispersions and columns represent different distances of the closest approach. Our best fit occurs for a stellar encounter with the minimum distance of 100–150 au and a velocity of $\sim$1 km s^{-1}. Resonant objects and classic Kuiper belt objects are included (pink triangles), and also scattered objects and Centaurs at radii less than 30 au (cyan crosses)

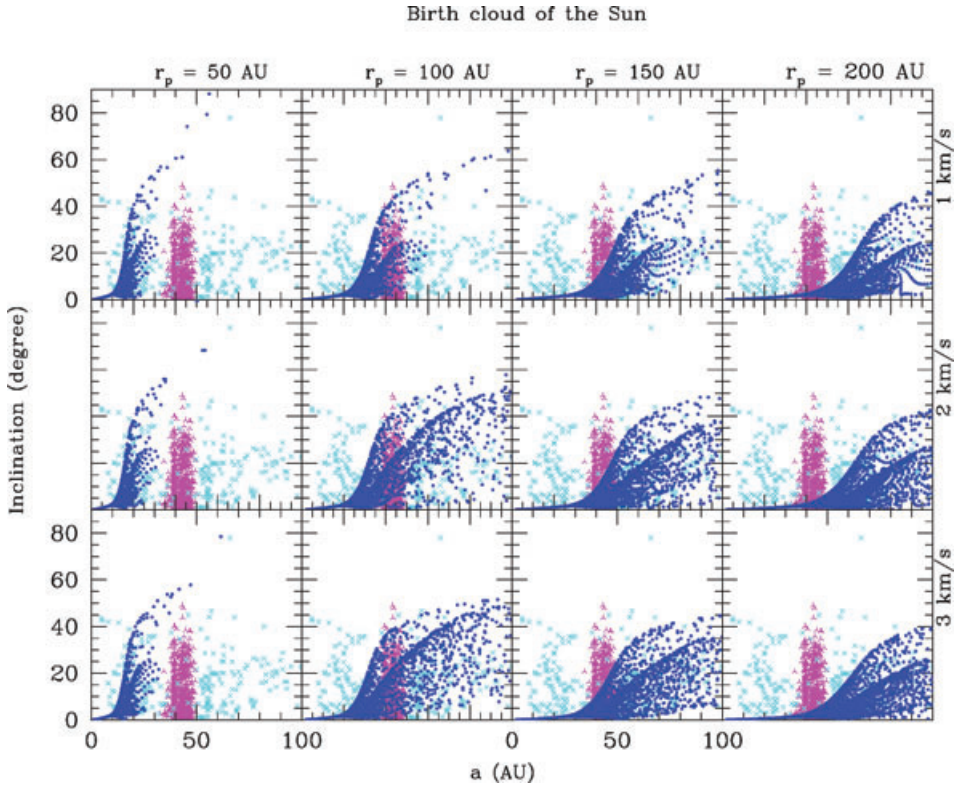

Figure 10. Same as Fig. 9 but for inclinations.

for which the effect caused by Gliese 710 would start to be notable is ∼300 au, producing a slight heating of the outer parts of the 100 au planetary disc, with eccentricities up to 0.1 on the semimajor axes between 60 and 100 au and inclinations up to 10°. With a simple impulse approximation we find that Gliese 710 will not even have an important effect on the global structure of the Oort Cloud.

For stars of the solar neighbourhood, with the known 6D information, we constructed orbits in order to compare the use of a simple straight-line approximation, a local approximation to the Galactic potential, an axisymmetric potential and a full Galactic potential (including spiral arms and bar observationally motivated). Even for times as short as 10 Myr, stars beyond ∼20 pc have significant differences in their trajectories for the different approximations, showing where the Galactic global potential becomes important. A local potential clearly does better than the straight-line approximation. Comparing the global potential model (including spiral arms and bar), with the simpler model of García-Sánchez et al. (2001) (that includes spiral arms), we find that 73 per cent of our trajectories differ by less than 3 per cent, and for the rest (the most distant stars in general) the errors are 6–26 per cent. Differences among stellar orbits due to the use of different models for the Galactic potential field or the simple straight-line approximation become more important the farer the star is, making even more uncertain approaches to the Sun in its path for the Milky Way disc. To compute precise stellar orbits of the solar neighbourhood, taking advantage of the new generation of data produced by large surveys, we will require better models of the Milky Way Galaxy instead of simpler approximations.

Finally, regarding the birth cloud of the Sun, we produced several experiments to reproduce the orbital parameters of the Kuiper belt objects. We know that at 42–48 au there are objects with eccentricities up to 0.4. We are able to approximate these objects using encounters with a velocity at infinity of 1 km s^{-1} and a close-approach distance of 100 au. This results in eccentricities from 0 to 0.1 on semimajor axis in the interval of 0–40 au, and eccentricities from 0 to 1 on the semimajor axis in the interval of 40–65 au and from 65 until 100 au the most of the particles are dynamically evaporated.

ACKNOWLEDGMENTS

We are grateful to the anonymous referee for valuable comments which contributed to improve the present paper. BP and JJ thank Antonio Peimbert, Justin Read and Prasenjit Saha, for enlightening discussions and Santiago Torres-Rodriguez for his help with the stellar catalogues. JJ and BP thank projects UNAM through grants PAPIIT IN110711-2 and IN-112210-2 and CONACYT through grant 60581.

REFERENCES

Adams F. C., 2010, ARA&A, 48, 47
Antoja T., Valenzuela O., Pichardo B., Moreno E., Figueras F., Fernández D., 2009, ApJ, 700, 78
Binney J., Tremaine S., 2007, Galactic Dynamics. Princeton Univ. Press, Princeton, NJ
Bobylev V. V., 2010, Astron. Lett., 36, 220
Bower G., Bolatto A., Ford E., Kalas P., 2009, ApJ, 701, 1922
Brasser R., Duncan M. J., Levison H. F., 2006, Icarus, 184, 59
Brasser R., Duncan M. J., Levison H. F., 2007, Icarus, 191, 413
Brasser R., Duncan M. J., Levison H. F., 2008, Icarus, 196, 274
Carpenter J. M., 2000, AJ, 120, 3139
Chakrabarty D., 2007, A&A, 467, 145
Clark P. C., Bonnell I. A., Zinnecker H., Bate M. R., 2005, MNRAS, 359, 809
de la Fuente Marcos C., de la Fuente Marcos R., 1997, A&A, 326, L21
Dehnen W., 2000, AJ, 119, 800
Dybczyński P. A., 2006, A&A, 449, 1233
Gaidos E. J., 1995, Icarus, 114, 258
García-Sánchez J., Preston R. A., Jones D. L., Weissman P. R., Lestrade J.-F., Latham D. W., Stefanik R. P., 1997, in Battrick B., ed., Proc. ESA Symp. Vol. 402, 'Hipparcos-Venice '97'. ESA Publications, Noordwijk, p. 617
García-Sánchez J., Preston R. A., Jones D. L., Weissman P. R., Lestrade J.-F., Latham D. W., Stefanik R. P., 1999, AJ, 117, 1042
García-Sánchez J., Weissman P. R., Preston R. A., Jones D. L., Lestrade J.-F., Latham D. W., Stefanik R. P., Paredes J. M., 2001, A&A, 379, 634
Gilmore G., 1992, in Maran S. P., ed., The Astronomy and Astrophysics Encyclopedia. Cambridge Univ. Press, Cambridge, p. 643
Goswami J. N., Vanhala H. A. T., 2000, in Mannings V., Boss A. P., Russell S. S., eds, Protostars and Planets IV. Univ. Arizona Press, Tuscon, p. 963
Hall S. M., Clarke C. J., Pringle J. E., 1996, MNRAS, 278, 303
Hester J. J., Desch S. J., Healy K. R., Leshin L. A., 2004, Sci, 304, 1116
Hills J., 1981, AJ, 86, 1730
Hurley J., Shara M., 2002, ApJ, 565, 1251
Ida S., Larwood J., Burkert A., 2000, ApJ, 528, 351
Kenyon S., Bromley B., 2004, Nat, 432, 598
Kirsh D., Duncan M., Brasser R., Levison H., 2009, Icarus, 199, 197
Kobayashi H., Ida S., 2001, Icarus, 153, 416
Lada C. J., Lada E. A., 2003, ARA&A, 41, 57
Laughlin G., Adams F. C., 1998, ApJ, 508, L171
Looney L., Tobin J., Fields B., 2006, ApJ, 652, 1755
Martos M., Hernandez X., Yáñez M., Moreno E., Pichardo B., 2004, MNRAS, 350, L47
Mathews R., 1994, QJRAS, 35, 1
Meyer B. S., Clayton D. D., 2000, Space Sci. Rev., 92, 133
Miyamoto M., Nagai R., 1975, PASJ, 27, 533
Morbidelli A., Levison H., 2004, AJ, 128, 2564
Pfahl E., Muterspaugh M., 2006, ApJ, 652, 1694
Pichardo B., Martos M., Moreno E., Espresate J., 2003, ApJ, 582, 230
Pichardo B., Martos M., Moreno E., 2004, ApJ, 609, 144
Press W. H., Teukolsky S. A., Vetterling W. T., Flannery B. P., 1992, Numerical recipes in FORTRAN. The art of scientific computing, 2nd edn. Cambridge Univ. Press, Cambridge
Schneider J., 2010, Extrasolar Planets Encyclopedia. http://exoplanet.eu/catalog-all.php
Spurzem R., Giersz M., Heggie D. C., Lin D. N. C., 2009, ApJ, 697, 458
Stern A., 2003, Nat, 424, 639
Udry S., Santos N. C., 2007, ARA&A, 45, 397
Wadhwa M., Amelin Y., Davis A. M., Lugmair G. W., Meyer B., Gounelle M., Desch S. J., 2007, in Reipurth B., Jewitt D., Keil K., eds, Protostars and Planets V. Univ. Arizona Press, Tuscon, p. 835
Weissman P., 1996, Earth Moon Planets, 72, 25

This paper has been typeset from a TEX/LATEX file prepared by the author.